

Effect of silver nanoparticles content on the various properties of nanocomposite hydrogels by in situ polymerization

Wen-Fu Lee · Kai-Tai Tsao

Received: 24 April 2009 / Accepted: 14 September 2009 / Published online: 30 September 2009
© Springer Science+Business Media, LLC 2009

Abstract A series of nanocomposite hydrogels (APEAg series gels) were prepared from acrylic acid, poly(ethylene glycol) methyl ether acrylate, and silver nanoparticles through in situ polymerization by UV irradiation. The effect of the content of silver nanoparticle on the properties of the nanocomposite hydrogels was investigated. Results showed that, with increasing of the content of the silver nanoparticle in the hydrogels, the crosslinking density and shear modulus of the hydrogel were not obviously changed, the electrical conductivities of the nanocomposite hydrogels increased, and their initial rate of *Escherichia coli* inactivation significantly increased, but their adhesive force only slightly decreased. These materials can be assessed as promising bioadhesive patch or wound-dressing material or electrical massage patch.

Introduction

Silver nanoparticles and silver colloids were extensively investigated in recent years because they have superior properties such as electrical conductivity and bactericidal action. Several methods were used to prepare silver nanoparticles, such as chemical reduction [1–3], photochemical or radiation-chemical reduction [4, 5], microwave-assisted [6], and sono-chemical method [7].

Polymer–metal nanocomposites can be obtained by two different approaches, namely, ex situ and in situ techniques. In the ex situ approach, nanoparticles are first produced by soft-chemistry routes and then dispersed into

polymeric matrices. In the in situ method, metal particles are generated inside a polymer matrix by decomposition or chemical reduction of a metallic precursor dissolved into the polymer [8]. For example, silver ions are successfully reduced and dispersed in poly(vinyl pyrrolidone) (PVP), poly(vinyl alcohol), and poly(2-hydroxyethyl methacrylate) matrices. Another method was used to prepare polymer–silver nanoparticle composites with γ -irradiation, in which reduction of Ag^+ and polymerization of monomer took place simultaneously [9, 10]. Zhang et al. [4] further improved the simultaneous polymerization–reduction method to prepare PAN/silver nanoparticle composite.

Bioadhesive is defined as the adhesion of a polymer and a biological structure. It is widely used in hard and soft tissue applications [11]. As a bioadhesive, polymer should have some properties such as strong hydrogen-bonding groups ($-\text{OH}$, $-\text{COOH}$), strong anionic charge (COO^- , SO_3^-), high molecular weight, sufficient chain flexibility, and surface energy favoring the spread onto mucus [12, 13]. In recent years, drug delivery systems using bioadhesive drug carriers have become increasingly important due to their ability to adhere to mucosal surfaces of the buccal and skin, thereby increasing therapeutic efficiency [14, 15]. Polymers using as mucoadhesive drug carriers include poly(acrylic acid) (PAA), poly(methacrylic acid), carboxymethyl cellulose, and hydroxypropyl methylcellulose [16, 17]. Among the investigated polymers, PAA and lightly crosslinked PAA are the best bioadhesive due to its hydrophilic nature, negative charge, and high flexibility [18].

A series of nanocomposite hydrogels (APECAG series gels) prepared from acrylic acid (AA), poly(ethylene glycol) methyl ether acrylate (PEGMEA), and silver nanoparticles through the ex situ polymerization were reported in a previous study [19]. The results showed that the silver

W.-F. Lee (✉) · K.-T. Tsao
Department of Chemical Engineering, Tatung University,
Taipei, Taiwan
e-mail: wflee@ttu.edu.tw

nanoparticles were embedded in the gels and this result lowered the electrical conductivity and *Escherichia coli* inactivation effect of the gels. To improve these effects, a simultaneous polymerization–reduction method (in situ polymerization) was adopted to prepare a series of nanocomposite hydrogels (APEAg series gels) from AA, PEGMEA, and silver nanoparticles by UV irradiation. The various properties of the nanocomposite hydrogels were investigated.

Experimental

Materials

Acrylic acid and diethoxyacetophenone (DEAP) as a photoinitiator were purchased from Fluka Chemical Co. (Buchs, Switzerland). PEGMEA ($M_n = 454$) and 1-vinyl-2-pyrrolidone (VP) were purchased from Aldrich Co. and Sigma Co. (St. Louis, MO), respectively. Silver nitrate (AgNO_3) was purchased from Nihon Shiyaku Industries, LTD (Osaka, Japan) and ethylene glycol dimethacrylate (EGDMA) used as a crosslinker was purchased from TCI (Tokyo, Japan). *Escherichia coli* (*E. coli*, ATCC 8739) was purchased from Food Industry Research and Development Institute (Taipei, Taiwan). Luria–Bertani (LB) medium and agar powder were purchased from Difco (Franklin Lakes, NJ). AA was purified by vacuum distillation at 29 °C/6 mmHg. Other chemicals were used as received.

Preparation of silver/VP precursor solution and silver composite hydrogels

To prepare $[\text{VP}/\text{Ag}^+]$ precursor solution, 1.0 g of VP dissolving in 100 mL of water was mixed with 100 mL of 100 ppm silver nitrate solution at room temperature for 12 h. Appropriate amount of the precursor solution was added into the monomer solution and then 1 mol.% EGDMA and 1 mol.% DEAP were added as crosslinker and photoinitiator, respectively. The mixture was then injected into the space between two glass plates with 2-mm silicone rubber spacer. Polymerization and reduction were simultaneously carried out by exposing the monomer solution to UV irradiation (full-wavelength, 600 W) for 2 h. The gel membrane was cut into disks, 10 mm in diameter, and immersed in an excess amount of deionized water for 3 days to remove residual components after the gelation was completed. The sample codes, yields, and equilibrium-swelling ratios of the nanocomposite gels are listed in Table 1. The sample codes APEAgX denote the times of 55.6 ppm silver ion in the feed composition. For

Table 1 Compositions and swelling ratios of the APEAg series hydrogels

| Sample code ^b | APE0 | APEAg1 | APEAg1.5 | APEAg2 | APEAg2.5 |
|---------------------------|------|--------|----------|--------|----------|
| AA (mol.%) | 90 | 90 | 90 | 90 | 90 |
| PEGMEA (mol.%) | 10 | 10 | 10 | 10 | 10 |
| EGDMA (mol.%) | 1 | 1 | 1 | 1 | 1 |
| (VP/Ag) ^a (mL) | – | | | | |
| Ag (ppm) ^a | – | 55.6 | 83.4 | 111.2 | 139 |
| DEAP (mol.%) | 1 | 1 | 1 | 1 | 1 |
| Conversion of Ag (%) | – | 84.5 | 79.8 | 78.3 | 86.2 |
| (ppm) | – | 46.9 | 66.5 | 87.0 | 119.8 |
| Yield (%) | 94.3 | 96.1 | 93.2 | 91.1 | 94.2 |
| <i>Q</i> (g/g) | 1.64 | 1.29 | 1.23 | 1.14 | 1.13 |

^a The precursor content is based on the total monomer weight

^b The sample codes APEAgX denote the times of 55.6 ppm silver ion in the feed composition, such as APEAg2.5 denote the 2.5 times of 55.6 ppm (139 ppm) silver ion in the feed composition

example, APEAg2.5 denotes the 2.5 times of 55.6 ppm (139 ppm) silver ion in the feed composition.

Measurement of the conversion of aqueous AgNO_3 into solid Ag

The feed compositions of the composite polymers were similar to those for the preparation of the composite hydrogels as above-mentioned, except the crosslinker was not added. The monomer solution was exposed to UV irradiation for 2 h to simultaneously carry out polymerization and reduction. To dissolve the gel, the obtained polymer was dissolved in 100 mL of 0.3 N $\text{HNO}_{3(\text{aq})}$ at 100 °C for 48 h. The concentration of silver was measured by using the atomic absorption spectrometry (AAS; Varian, model 3000) with a calibration curve of silver prepared in advance.

X-ray diffraction analysis

Powder X-ray diffraction (XRD) analyses were performed with a MAC Science X-ray powder diffractometer, with Cu anode (model XRD-6000, Osaka, Japan), running at 40 kV and 30 mA and scanning from 10° to 80° at 3°/min. The $\text{AgNO}_{3(\text{aq})}$ was irradiated by UV for 2 h, and then centrifuged for 2 h. The precipitated silver particles were dried at 70 °C for 24 h. A portion of silver particles used as pristine sample was examined with XRD immediately. The other portions were examined after 3 months. Two series of xerogels were tiled on the cell to examine their XRD patterns.

Measurement of the equilibrium-swelling ratio

The pre-weighed dried gels (W_d) were immersed in deionized water at 25 °C until the swelling equilibrium was attained. Each gel was removed from the water bath, tapped with delicate task wipers to remove excess surface water, and weighed as the wet weight of the gel (W_w). The swelling ratio (Q) was calculated from the following equation:

$$Q = (W_w - W_d)/W_d. \tag{1}$$

Measurement of the swelling kinetics

The swelling ratio was obtained by weighing the initial and swollen samples at various time intervals. The amount of water absorbed, W_t , and the equilibrium water absorption at infinitely long time, W_∞ , were used to calculate the diffusion coefficient D with Eq. 2 for $W_t/W_\infty \leq 0.8$ [20]:

$$W_t/W_\infty = (4/\pi^{0.5})(Dt/L^2)^{0.5}, \tag{2}$$

where t is the time and L the initial thickness of the dried gel. To investigate the diffusion model of the gel, the initial swelling data were fitted with the exponential heuristic equation for $W_t/W_\infty \leq 0.6$ [21, 22]:

$$W_t/W_\infty = Kt^n, \tag{3}$$

where K is a characteristic constant of the gel and n a characteristic exponent of the mode transport of the penetrate. In addition, the penetration velocity (v) of water in each gel, which was described by Peppas et al., was determined with Eq. 4 [23, 24]:

$$v = \frac{1}{2\rho_w A} \left(\frac{dw}{dt} \right), \tag{4}$$

where $\frac{dw}{dt}$ is the slope of the weight gain versus time curve, ρ_w the density of water, A the surface area of one side of the disk, and factor 2 accounts for the fact that penetration takes place through both sides of the disk.

Measurement of the physical properties

The strengths of these hydrogels were measured by uniaxial compression experiment with Universal Tester (LLOYD LRX; J. J. Lloyd, Poole, UK). Equation 5 was used to calculate the shear modulus (G) [25, 26]:

$$\tau = F/A = G(\lambda - \lambda^{-2}), \tag{5}$$

where τ is the compression stress, F the compression load, A the cross-sectional area of swollen gels, and λ the compression strain. At low strains, a plot of τ versus $-(\lambda - \lambda^{-2})$ would yield a straight line whose slope is G . The effective crosslink density (ρ_x) can be calculated from the G and polymer volume fraction (v_2) with following Eq. 6:

$$\rho_x = G/v_2^{1/3}RT, \tag{6}$$

where R is the ideal gas constant and T the absolute temperature.

Assessment of adhesive force

The force detection system consists of a precision load cell and a roller with Universal Tester (LLOYD LRX). The nanocomposite gels were cut into the dimension of 3 cm by 1 cm (thickness: 2.0 mm), and brought in contact with PET film on the roller. Peel strength was determined with a constant speed of 30 mm/min and the force required to fracture the adhesive bond was recorded.

Measurement of electrical conductivity

A NAPSON four-point probe measurement was used for the sheet surface resistance study. The dry and wet hydrogels were cut into the dimension of 2 cm by 2 cm (thickness: 2.0 mm). The voltage (V) was measured under the given current (I), then Eqs. 7 and 8 were used to obtain sheet surface resistance (R_s) and resistivity (ρ) [27, 28]:

$$R_s \left(\frac{\Omega}{\text{sq}} \right) = \frac{\pi}{\ln 2} \times \frac{V}{I} = 4.532 \times \frac{V}{I}, \tag{7}$$

$$R_s \times d(\text{thickness}) = \rho(\text{resistivity}). \tag{8}$$

The data were the average of three or four points in the test.

Bacterial culture

Luria–Bertani agar is consisted of LB medium and 15 g/L of agar. Media and saline solutions were autoclaved at 121 °C for 15 min for sterilization. *E. coli* was preserved on LB agar. A loop of bacterial cells was inoculated to 100 mL LB medium in a 500-mL Erlenmeyer flask. This was cultured in a 37 °C incubator at 170 rpm for 12–16 h. The resultant culture was used for the following experiment.

Assay of antibacterial activity

One gram of hydrogel was broken into fragments and then put into 500-mL Erlenmeyer flasks with 100 mL sterile water. 1.0 mL of the bacterial culture was added into above-mentioned flask, the flasks were incubated in a 37 °C shaker. The samples were removed at 20, 40, 60 and 120 min, respectively. Samples were stepwise diluted by 10^3 - and 10^5 -fold with 0.85% saline solutions. The LB agar solution was sterilized and cooled in 50 °C water bath. The LB agar was then poured into Petri dishes (about 15 mL per Petri dish) containing 1.0 or 0.1 mL of the diluted samples. After thorough mixing of the bacterial dilutions

and agar media by gentle shaking, the agar media were stand for solidification. Colonies developed on the agar plates after incubation at 37 °C for 2 days were counted. The viabilities were determined by the pour plate method. The inactivation of *E. coli* was evaluated by comparing the change in viability during the incubation in the shake flask culture. The viability was presented by log CFU per mL.

Results and discussion

Effect of chelates formation conditions on silver particle size

The different concentrations of silver nitrate in VP solution were designed, the $[\text{VP-Ag}^+]$ chelates were formed under different stirring rates at 30 °C for 12 h. The formed chelates solutions were reduced by UV irradiation for 2 h. The silver nanoparticles were measured with particle size analyzer (HORIBA, LB-500). Figure 1 indicates that the silver particle size increases with an increase of the concentration of silver nitrate solution in VP. The increase of particle size maybe resulted from the aggregation of silver particles due to the absence of stabilizer such as PVP in chelate solution when the concentration of $\text{AgNO}_{3(\text{aq})}$ increased. The results also showed that the silver particle size was significantly affected by stirring rate, especially at low Ag^+/VP ratio. Table 1 showed that the conversion of $[\text{VP-Ag}^+]$ chelates under UV irradiation ranged from 78.3 to 86.2%.

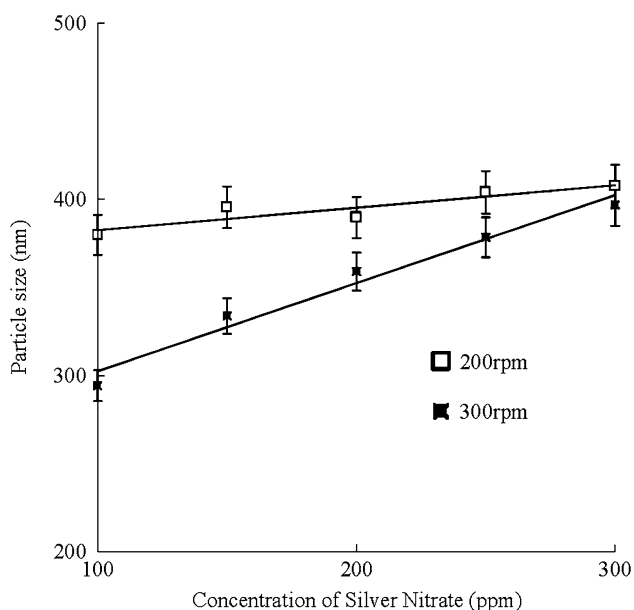


Fig. 1 Effect of stirring rate on the silver particle size under different concentrations of silver nitrate solution at 30 °C

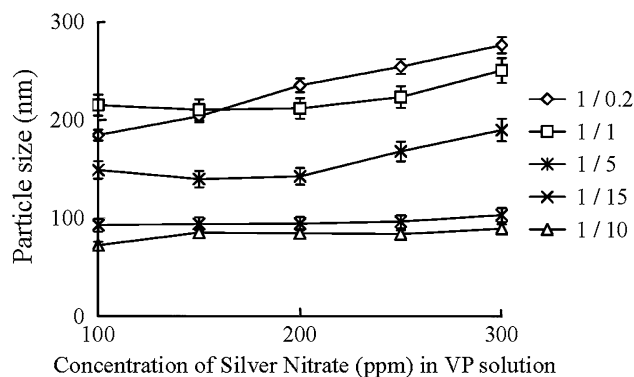


Fig. 2 Mean silver particles size against different AgNO_3/VP concentration ratios under stirring with 300 rpm at 30 °C and reduced by UV irradiation

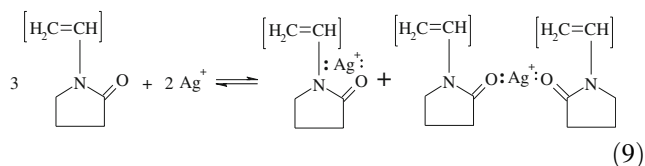
Effect of VP content on silver nanoparticle size

The effect of VP content on silver nanoparticles size was investigated under the condition of $[\text{VP-Ag}^+]$ chelate formation at 300 rpm and 30 °C. Figure 2 shows the effect of different silver nitrate concentrations on silver particle size under different AgNO_3/VP weight ratios. It can be found that the silver particle size increase with increasing of silver nitrate concentration under higher AgNO_3/VP weight ratio, but the silver particle size almost kept constant at lower AgNO_3/VP weight ratio (1/10 or 1/15). This is because the dynamic viscosity of $\text{AgNO}_{3(\text{aq})}$ increased when VP was added, that resulted in decreasing of silver ion aggregation, and consequently improved the silver ion dispersion. But, when the weight ratio of AgNO_3/VP approaches 1/10, the excess VP could chelate dispersible silver ions and formed the smallest nanoparticle size (72 nm) [29, 30]. This is well known that the PVP was usually used as protecting agent in the formation of silver nanoparticles.

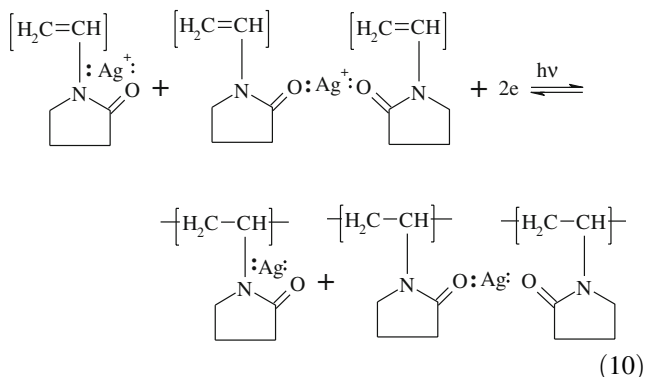
Mechanism of synthesis

Hartley [31] reported that silver ions can reversibly react with some olefin molecules to form silver–olefin complexes. Olefin molecules can donate their π -electrons from the occupied $2p$ orbitals to empty s orbitals of silver ions to form σ -bonds. The back donation of electron density from occupied d orbitals of silver ions into the empty π^*-2p antibonding orbitals of olefin molecules lead to the formation of π -bonds. Hong et al. [32] reported that silver cations form complexes with oxygen atoms of the carbonyl groups up to 1:1 mole ratio, above which the silver ion pairs and ion aggregates start to form. According to Zhang's report [29], the process of silver ions coordinating with VP monomers can be described as follow. The donated lone pairs of both nitrogen and oxygen atoms in

the polar group of VP may occupy two *sp* orbitals of the silver ion to form a complex compound. Also, because *sp* orbitals form a linear coordinative bond, 2 mole VP and 1 mole silver ion may form 1 mole complex. If the two kinds of possibility were equal, the reaction of VP and silver ion may be as in Eq. 9.



The reversible and specific reaction makes VP monomer be a carrier of silver ions, which provides an excellent precursor to synthesize in situ silver nanoparticles. When the solution was irradiated by ultraviolet, the polymerization of VP monomer was induced by photoinitiator. At the same time, the coordinating Ag^+ was reduced into metallic silver by photochemical reaction as Eq. 10.



The UV-absorbance spectra for the VP monomer and different [VP– Ag^+] solutions are shown in Fig. 3. The results show the maximum absorbance peaks shifted 2 nm from 231 nm for VP monomer to 233 nm for [VP– Ag^+] complex.

Identification of the silver particles

The silver particles show the XRD diffraction peaks with 2θ values of 38° , 44° , 64° , and 78° , corresponding to crystal faces of (111), (200), (220), and (311) for the face-centered cubic (fcc) crystalline silver (see Fig. 4a), and has a lattice parameter of 0.4089 nm. This result conforms to the reported data from JCPDS File No. 4-0783 [4]. The XRD pattern of APE0 gel (Fig. 4c) only shows a broad peak at 22° , but APEAg2.5 gel (Fig. 4b) displays a similar pattern as that of silver nanoparticles in Fig. 4a. This evidence shows that the [VP– Ag^+] complex can be successfully reduced to silver particle under in situ polymerization.

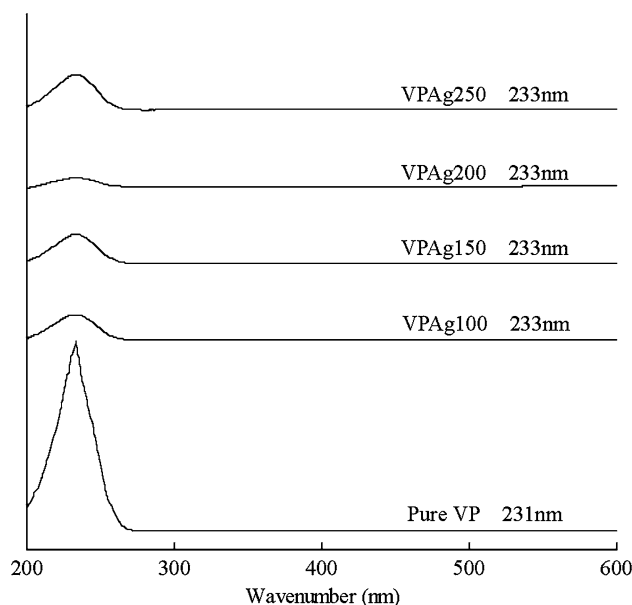


Fig. 3 UV absorbance for VP and silver ion chelate at different concentrations of precursor solution

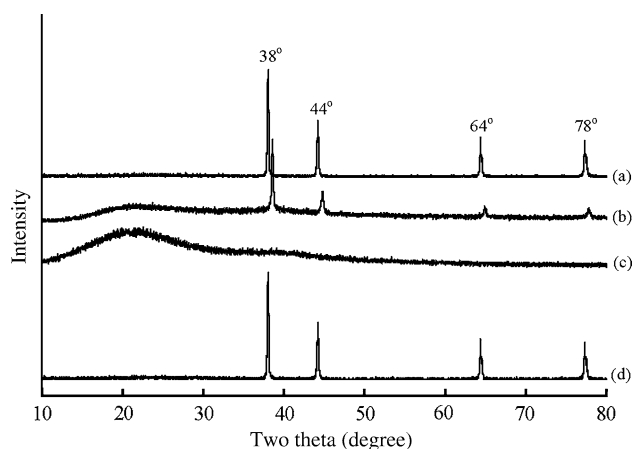


Fig. 4 XRD patterns of (a) silver nanoparticles, (b) APEAg2.5, (c) APE0, and (d) aging after 3 months

To check whether the silver nanoparticles were oxidized to silver oxide (Ag_2O), the XRD patterns for the pristine silver particle and the silver particle storing for 3 months under ambient condition were measured. The results in Fig. 4d exhibited that the same XRD patterns for all sample particles were observed, this result indicates that the silver nanoparticles are stable under ambient condition.

Effect of silver nanoparticle content on swelling kinetics

The swelling ratios as a function of time for the different composite hydrogels in deionized water at 25°C are shown in Fig. 5. The results show that the equilibrium-swelling

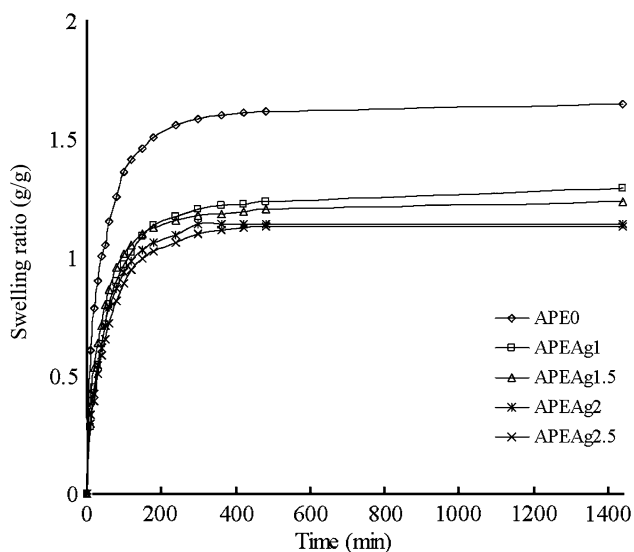


Fig. 5 Swelling ratio as a function of time for APEAg hydrogel in deionized water at 25 °C

ratio decreases with an increase of silver content in the composite (also see Table 1). The equilibrium-swelling ratio from 1.64 g/g for APE0 gel decreases 21.3% to 1.29 g/g for APEAg1 gel, and then slowly decreases 31.1% to 1.13 g/g for APEAg2.5 gel.

The initial swelling kinetics of the nanocomposite hydrogels are shown in Table 2. The results indicate that both the diffusion coefficient of water, D , and the penetration velocity of water into the gel, v , decrease with an increase of the silver nanoparticle content in the gels. The D and v values at initial swelling period from 7.05×10^{-7} (cm/s²) and 0.33 (cm/min) for APE0 gel sharply decrease

Table 2 The kinetic characteristic for the composite hydrogels with various silver nanoparticle contents

| Sample code | $D \times 10^7$ (cm/s ²) | v (cm/min) |
|-------------|--------------------------------------|--------------|
| APE0 | 7.05 | 0.329 |
| APEAg1 | 2.12 | 0.252 |
| APEAg1.5 | 1.69 | 0.229 |
| APEAg2 | 1.66 | 0.21 |
| APEAg2.5 | 1.34 | 0.201 |

Table 3 Physical properties of the APEAg series hydrogels

| Sample code | $\rho_x \times 10^5$ Wet gel (mol/cm ³) | G (g/cm ²) | Adhesive force (g/cm ²) |
|-------------|---|--------------------------|-------------------------------------|
| APE0 | 1.74 ± 0.05 | 218.63 ± 16 | $16.73 \pm 0.3\%$ |
| APEAg1 | 1.78 ± 0.01 | 235.16 ± 19 | $16.32 \pm 1.6\%$ |
| APEAg1.5 | 1.82 ± 0.02 | 240.82 ± 23 | $16.22 \pm 1.3\%$ |
| APEAg2 | 1.83 ± 0.05 | 243.44 ± 14 | $15.61 \pm 0.7\%$ |
| APEAg2.5 | 1.85 ± 0.01 | 248.38 ± 27 | $14.99 \pm 0.2\%$ |

70 and 23.4% to 2.12×10^{-7} (cm/s²) and 0.252 (cm/min) for APEAg1 gel, respectively. However, when the more silver particle was added, these two values slowly decrease from 76.0 and 30.4% for APEAg1.5 gel to 81 and 38.9% for APEAg2.5 gel. These results can be interpreted from two view-points. The major one reason is the anionic carboxylate charges ($-\text{COO}^-$) were neutralized by the unchelated silver ions. This occurrence resulted in decreasing the repulsion among anionic carboxylate groups. The other reason we thought is the silver nanoparticle in the gel reduced from silver ion would occupy the mesh space or pore volume of the gel network that resulted in the decrease of the swelling ratio of the gel. These reasons diminish the rate of water to diffuse or penetrate into the gel. Similar results were observed from our previous study in the ex situ polymerization of APEAg gel [19].

Comparing v and D for the APEAg and APEAg two series hydrogels, the penetration velocities of the APEAg series hydrogels are relatively larger than those of the APEAg series hydrogels. The denser and smoother surface of the APEAg series hydrogels may contribute to block the water to penetrate into the interior of gels (also see Fig. 8f).

Effect of silver nanoparticle content on gel strength and adhesive force

The gel strength can be assessed by the shear modulus (G) obtained from Eq. 5. The results in Table 3 indicate that the G values of the gels increase from 218.63 to 248.38 (g/cm²) with increasing silver nanoparticle content. The effective crosslink density (ρ_x) is defined as the concentration of elastically active chain (chain are deformed by an applied active stress) in the polymer network and is usually reported on the basis of moles of chain per cubic centimeter of dry polymer. The ρ_x values for the present gels are listed in Table 3. The results indicate that the ρ_x values increase from 1.74 to 1.85×10^{-5} (mol/cm³) with increasing silver nanoparticles in the gel. These results imply that the incorporation of the silver nanoparticles into the gel can enhance the gel strength and the chemical crosslink between the polymer matrices. These results are similar to our previous results in a series of APEAg gels [19].

The adhesive force was determined by measuring the force required to break the adhesive surface between the substrate (PET film) and the gels. The measured adhesive forces of the nanocomposite hydrogels are listed in Table 3. The adhesive forces for the present gels decrease from 16.73 to 14.99 g/cm² with an increase of silver nanoparticles in the gel, but for the previous APECaG series gels, their adhesive forces decreased from 16.73 to 15.81 g/cm² [19]. These results explicitly suggested that the silver particles produced by in situ polymerization would more easily hamper the adhesive properties of carboxylic group on the surface of the APEAg series gels.

Effect of silver nanoparticles content on electrical resistivity

The electrical resistivities of the APEAg series gels with various contents of silver particles are listed in Table 4. The results show that the electrical resistivities of gels decrease with increasing silver content in both the dry and wet gels. However, there is no significant difference between dry and wet gels with the same silver content. The electrical resistivities for APE0 gel in different swelling times are listed in Table 5. The results show that the surface electrical resistivities of the gels decrease with an increase of water content. The silver nanoparticles dispersed on the APEAg hydrogels surface contribute to the increase of electrical conductivity. Comparing the electrical resistivities between APEAg and APECaG series hydrogels, the electrical resistivities of APEAg are much lower (1,195 Ω cm for APEAg2.5) than those of APECaG

Table 4 Electrical resistivity of the APEAg series hydrogels

| Sample code | Dry hydrogel ρ (Ω cm) | Wet hydrogel ρ (Ω cm) |
|-------------|--|---------------------------------|
| APE0 | 3.0 × 10 ¹⁰ ± 1.2 × 10 ⁹ | 24872.5 ± 3.8 × 10 ³ |
| APEAg1 | 1786.8 ± 285 | 1742.7 ± 237 |
| APEAg1.5 | 1604.7 ± 254 | 1584.1 ± 218 |
| APEAg2 | 1579.3 ± 220 | 1516.9 ± 203 |
| APEAg2.5 | 1195.7 ± 192 | 1342.4 ± 187 |

Table 5 Electrical resistivity of the APE0 hydrogel in different swelling times

| Sample code | Wet hydrogel ρ (Ω cm) |
|--------------|--|
| APE0-0 mins | 3.0 × 10 ¹⁰ ± 1.2 × 10 ⁹ |
| APE0-5 mins | 1.66 × 10 ⁷ ± 2.1 × 10 ⁴ |
| APE0-10 mins | 3.39 × 10 ⁶ ± 8.9 × 10 ³ |
| APE0-15 mins | 2.65 × 10 ⁶ ± 8.7 × 10 ³ |
| APE0-20 mins | 1.64 × 10 ⁶ ± 8.8 × 10 ³ |
| APE0-25 mins | 4.46 × 10 ⁵ ± 8.4 × 10 ³ |

series hydrogels (2.5 × 10⁸ Ω cm for APECaG2.5). That is, the electrical conductivities for APEAg gels are much higher than those for APECaG gels. This is due to the silver nanoparticles almost entrapped inside the APECaG gels [19].

Effect of silver nanoparticle content on *E. coli* inactivation

It is well known that silver nanoparticle have a bacterial inactivation and anti-inflammation effect. Figure 6 shows the tendency of the bactericidal efficiency against *E. coli* for the APEAg gels. The order of bactericidal effect is APEAg2.5 > APEAg2 > APEAg1.5 > APEAg1 > APE0, suggesting bactericidal activity increases with an increase in silver nanoparticle content in the composite gels.

Effect of silver nanoparticle content on the first-order destruction of *E. coli*

The effect of the silver nanoparticle content on the first-order destruction of the bacteria was evaluated. The expression of the first-order response can be given as following equation:

$$-\frac{dN}{dt} = kN, \tag{11}$$

where $-dN/dt$ is the rate of concentration decrease, N the concentration of viable microorganisms, and k the rate constant of first-order reaction. The initial rate constant of bacterial inactivation as a function of silver content in APEAg gels was shown in Fig. 7. The inactivity effect was approximately linear with the silver content ranging from 55.6 to 139 ppm, in contrast to that ranges from 28.6 to

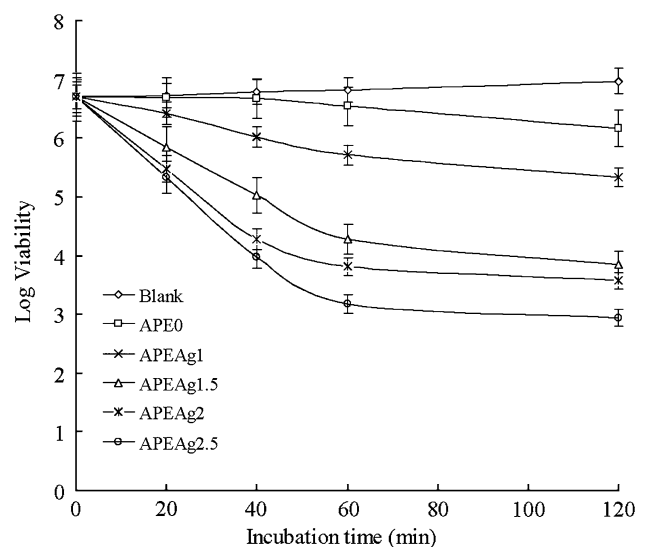


Fig. 6 Inactivation of *E. coli* as a function of incubation time for the APEAg series hydrogel in shake flask culture

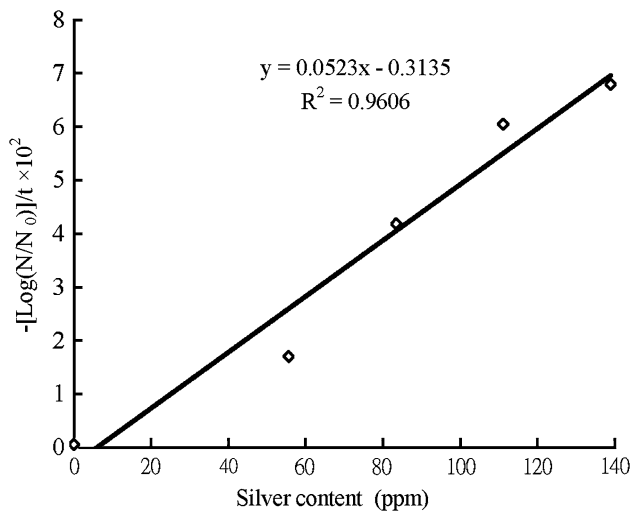
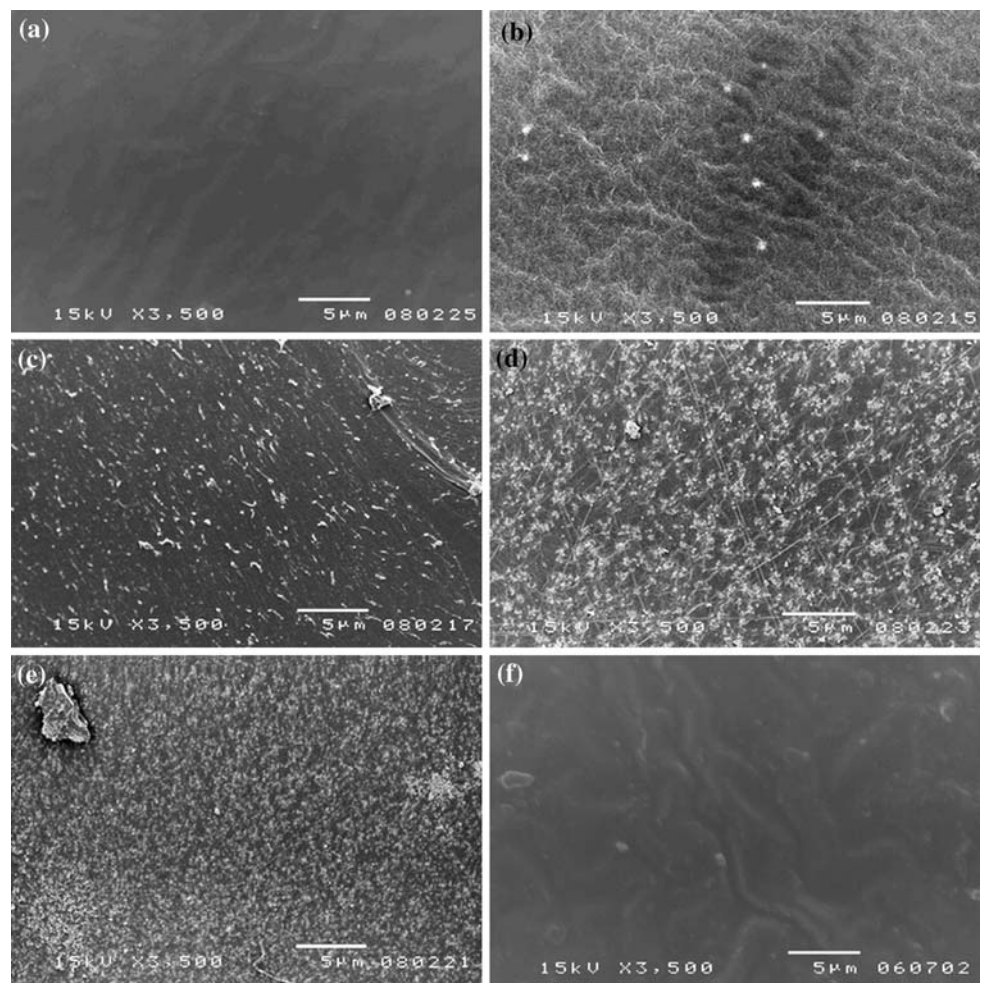


Fig. 7 Initial rate of bacterial inactivation as a function of silver content for the APEAg series hydrogel

71.9 ppm for the APECAG series gels [19], the contents of silver nanoparticles were higher in APEAg series gel and those nanoparticles were dispersed on the hydrogel surface.

Fig. 8 SEM surface microphotographs for the APEAg hydrogels **a** APE0, **b** APEAg1, **c** APEAg1.5, **d** APEAg2, **e** APEAg2.5, and **f** APECAG2.5



Hence, the bactericidal contact areas of silver particles for APEAg gels were wider and larger, resulting in a better bacterial inactivation.

SEM

To observe the surface morphology of the gels, the surface microphotographs for a series of nanocomposite hydrogels were measured with SEM and shown in Fig. 8. The number (white point shown in Fig. 8b–e) of silver nanoparticles increased with an increase of the silver content in the gels and those were well dispersed on the surface of hydrogels. The surfaces of the gels were coarser with an increase of the silver content in the gels. Comparing Fig. 8a, e, and f, we also found that the surfaces of the APE0 gel and APECAG2.5 gel were smoother than that of APEAg series gel. These results supported that why the electrical conductivity and bactericidal efficiency increased with an increase in silver nanoparticle content in the gels; and confirmed that why the initial D and v values for APECAG series gels were lower than those of APEAg gels.

Conclusions

Poly(AA-co-PEGMEA)/silver nanoparticle composite hydrogels were successfully synthesized. The XRD patterns showed that the silver nanoparticle could be prepared through in situ polymerization. The surface microphotographs showed that the silver nanoparticles can be successfully well dispersed onto the surface of the gels. The increase of the silver nanoparticle content resulted in lowering swelling ratio of the gels, which is supported by the results of lower diffusion coefficient and the penetration velocity of water through gel. The presence of silver nanoparticles in the gel composition could increase the gel strength and crosslinking density of the gel. Although their adhesive forces slightly decreased with increase in silver nanoparticles, the APEAg series hydrogel showed a good electrical conductivity and a perfect antibacterial efficiency.

Acknowledgements The authors wish to thank the National Science Council of the Republic of China for financial support under Grant NSC 93-2216-036-01. The authors also appreciated professor Dey-Chyi Sheu (Department of Bioengineering) for his excellent skillful assistance and discussion in bacterial inactivation.

References

- Nersisyan HH, Lee JH, Son HT, Won CW, Maeng DY (2003) *Mater Res Bull* 38:949
- Sondi I, Goia DV, Matijevic E (2003) *Colloid Interface Sci* 260:75
- Chou KS, Ren CY (2000) *Mater Chem Phys* 64:241
- Zhang Z, Zhang L, Wang S, Chen W, Lei Y (2001) *Polymer* 42:8315
- Liu H, Ge X, Ni Y, Ye Q, Zhang Z (2001) *Rad Phys Chem* 61:89
- Liu FK, Huang PW, Chang YC, Ko FH, Chu TC (2004) *J Mater Res* 19:469
- Okitsu K, Bandow H, Maeda Y (1996) *Chem Mater* 8:315
- Carotenuto G, Nicolais L, Martorana B, Perlo P (2005) In: Nicolais L, Carotenuto G (ed) *Metal-polymer nanocomposites: metal-polymer nanocomposite synthesis: novel ex situ and in situ approaches*, chap 5. Wiley Interscience, New York, p 155
- Zhu YJ, Qian YT, Li XJ, Zhang MW (1998) *Nanostruct Mater* 10:673
- Zhu YJ, Qian YT, Zhang MW, Chen ZY, Bin L, Wang CS (1993) *Mater Lett* 17:314
- Shojaei AH, Li X (1997) *J Control Release* 47:151
- Mortazavi SA (1995) *Int J Pharm* 124:173
- Chickering DE, Mathiowitz E (1995) *J Control Release* 34:251
- Florence AT, Jani PU (1994) *Drug Saf* 10:233
- Hwang SJ, Park H (1998) *Crit Rev Ther Drug Carrier Syst* 15:243
- Ahuja A, Khar RK, Ali J (1997) *Drug Dev Ind Pharm* 23:489
- Yang XJ, Robinson R (1998) In: Okano T (ed) *Biorelated polymers and gel: controlled release application in biomedical engineering*. Academic Press, London, p 135
- Park H, Robinson JR (1987) *Pharm Res* 4:457
- Lee WF, Tsao KTJ (2006) *Appl Polym Sci* 5:3653
- Kabra BG, Gehnke SW, Hwang STJ (1991) *Appl Polym Sci* 42:2409
- Franson NM, Peppas NAJ (1983) *Appl Polym Sci* 28:1299
- Korsmeyer RW, Merrwall EW, Peppas NA (1986) *J Polym Sci Polym Phys Ed* 24:109
- Peppas NA, Franson NM (1983) *J Control Release* 21:983
- Davidson CW, Peppas NA (1986) *J Control Release* 3:259
- Peppas NA, Barr-Howell BD (1986) *Hydrogels in medicine and pharmacy*, vol 1. CRC Press, Boca Raton, p 27
- Treloar LRG (1975) *The physics of rubber elasticity*. Clarendon Press, Oxford
- Valdes LG (1954) *Proc IRE* 42:420
- Smits FM (1958) *Bell Syst Tech J* 37:711
- Zhang Z, Zhao B, Hu L (1996) *J Solid State Chem* 121:105
- Bredas JL, Silbey R (1991) *Conjugated polymers*. Kluwer Academic Publisher, Dordrecht, p 49
- Hartley FR (1973) *Chem Rev* 73:163
- Hong SU, Jin JH, Won J, Kang YS (2000) *Adv Mater* 12:968